CHIN. PHYS. LETT. Vol. 34, No. 7 (2017) 076201

LaB_6 Work Function and Structural Stability under High Pressure *

Peng-Shan Li(李鹏善)[1,2], Wei-Ran Cui(崔巍然)[1,2], Rui Li(李蕊)[1], Hua-Lei Sun(孙华蕾)[1], Yan-Chun Li(李延春)[1], Dong-Liang Yang(杨栋亮)[1], Yu Gong(宫宇)[1], Hui Li(李晖)[3]**, Xiao-Dong Li(李晓东)[1]**

[1]*Institute of High Energy Physics, Chinese Academy of Sciences, Beijing 100049*
[2]*University of Chinese Academy of Sciences, Beijing 100049*
[3]*Institute of Microstructure and Properties of Advanced Materials, Beijing University of Technology, Beijing 100124*

(Received 10 March 2017)

The work functions of the (110) and (100) surfaces of LaB_6 are determined from ambient pressure to 39.1 GPa. The work function of the (110) surface slowly decreases but that of the (100) surface remains at a relatively constant value. To determine the reason for this difference, the electron density distribution (EDD) is determined from high-pressure single-crystal x-ray diffraction data by the maximum entropy method. The EDD results show that the chemical bond properties in LaB_6 play a key role. The structural stability of LaB_6 under high pressure is also investigated by single-crystal x-ray diffraction. In this study, no structural or electronic phase transition is observed from ambient pressure to 39.1 GPa.

PACS: 62.50.−p, 61.05.cp, 65.40.gh, 71.20.Ps DOI: 10.1088/0256-307X/34/7/076201

LaB_6 is one of the most important cathode materials in high-power electronics technology.[1] It has high electrical conductivity, high thermionic electron emission with a low work function, high brightness, and long-life properties compared with conventional tungsten filaments.[2] All of these interesting properties are related to the crystal structure and electronic properties, particularly the chemical bond characteristics. Pressure can greatly influence the material properties of LaB_6. Many theoretical and experimental works on the structural[3–9] and electronic[10–16] properties have been reported. However, there have been few studies of the work function under pressure. Furthermore, the results of the structural stability of LaB_6 are contradictory and insufficient. The measurements of Teredesai *et al.*[6] showed evidence of LaB_6 undergoing an electronic phase transition from cubic (space group $Pm\bar{3}m$) to orthorhombic ($Pban$) phase around 10 GPa, which is consistent with their Raman results. However, in the work of Godwal *et al.*,[17] no sign of phase transition was observed for either x-ray diffraction study or the Raman scattering experiment up to 25 GPa. In previous high-pressure diffraction experiments, the powder x-ray diffraction method has been widely used. However, the powder diffraction method has some shortcomings, such as uniaxial-stress-related peak broadening, a preferred orientation, and peak overlap of the sample and pressure medium peaks. The powder diffraction method is limited for resolving subtle structural distortions, such as the suggested $Pm\bar{3}m \rightarrow Pban$ transition in LaB_6,[6] also it is difficult to determine the accurate electron density distribution (EDD). It is known that the single-crystal diffraction method overcomes these shortcomings and it is far superior for distinguishing the phase transition and determining the EDD.

In this work, we investigate the characteristics of the work function of LaB_6 under high pressure and confirm the structural stability by the high-pressure single-crystal x-ray diffraction (HPSXD) method. According to the Fermi–Dirac theory, the charge density distribution will affect the Fermi energy. Based on the definition, the work function is determined by the Fermi energy. Therefore, if the precise electron density distribution can be determined under different pressures, the relationship between the work function and the pressure can be determined. Using the maximum entropy method (MEM),[18] we determine the EDD from single-crystal diffraction data and investigate the properties of the chemical bonds in LaB_6.[19–21] Furthermore, we calculate and investigate the changes in the bonds[20] and work function of LaB_6.

The LaB_6 sample was synthesized by the zone melting method. The HPSXD experiment was performed at the 4W2 beamline of the Beijing Synchrotron Radiation Facility.[22,23] A specially designed single-crystal diamond anvil cell with a large opening angle of $4\theta = 60°$ was used. The culet diameter of the anvil was 250 μm. A 250-μm-thick stainless steel gasket was pre-indented to 30 μm, and a 70 μm diameter sample chamber was drilled. The 25 μm thick single-crystal LaB_6 was cut to about 20 μm×20 μm and loaded in the sample chamber. A small ruby chip was loaded for the pressure measurements.[24] Neon was loaded into the sample chamber as the pressure transmitting medium. An MAR345 image-plate detector was set 186.5 mm away from the sample, which ensured that the data resolution was higher than 0.85 Å. The beam wavelength was 0.6199 Å (20 keV), which is 50 μm×50 μm full width at half maximum (FWHM) in both the horizontal and vertical directions. The single-crystal diffraction data were collected and analyzed by the HPSXD software package.[25] During the experiments, the sample was rotated in 2° steps

*Supported by the National Natural Science Foundation of China under Grant Nos 11274030 and 11474281.
**Corresponding author. Email: lixd@ihep.ac.cn; huilicn@yahoo.com
© 2017 Chinese Physical Society and IOP Publishing Ltd

from −25° to 25°, giving 25 patterns at each pressure. In each 2° step, the sample was continuously exposed with a constant rotation speed. For the HPSXD diffractogram, we used the HPSXD package to obtain the orientation matrix and the SHELX[26] format data file (hkl) to perform structure solution and refinement. During the HPSXD experiments, the sample size was considerably smaller than a normal laboratory diffraction sample and covered by the x-ray beam during the experiment. The sample absorption effect on the relative intensity was calculated to be less than 5%, which could be ignored.

The maximum pressure was 39.1 GPa in this work. There was no peak splitting or new peak production during the experiments. This means that there was no crystal structure phase transition and the space group $Pm\bar{3}m$ (No.221) remained unchanging.

In the LaB_6 unit cell, one lanthanum atom is located at the (0, 0, 0) site and the six boron atoms are located at (z, 0.5, 0.5) sites, where z is an internal parameter that determines the ratio between the inter- and intra-octahedron B–B distances. With increasing the pressure, the lattice parameter gradually decreases. However, the internal parameter z is almost unchanged (Fig. 2(d)). This means that the positions of the boron atoms remain stable during the experiment. The structure refinement results are listed in Table 1.

Table 1. Lattice parameters and structure refinement parameters at selected pressure points.

Pressure (GPa)	0.1 MPa[a]	4.6	6.9	13.1	17.4
Lattice parameters (Å)	4.1581(3)	4.1235(4)	4.1086(5)	4.0683(4)	4.0446(5)
B position z	0.2007(26)	0.2001(28)	0.1998(41)	0.1995(22)	0.1988(21)
Reflections collected/unique	120/23	55/20	51/20	51/19	51/20
Rint	0.0441	0.0452	0.0507	0.0255	0.0280
Completeness (%)	100	90.9	90.7	86.4	90.9
Data/restraints/parameters	23/0/5	20/0/5	20/0/5	19/0/5	20/0/5
Goodness-of-fit on F^2	1.270	1.382	1.281	1.208	1.228
Final R indices R1	0.0112	0.0154	0.0253	0.0119	0.0131
wR2	0.0291	0.0350	0.0620	0.0254	0.0289
Largest diff. peak and hole (e/Å^3)	0.37/−0.34	0.40/−0.91	0.28/−0.78	0.26/−0.52	0.30/−0.68
Pressure (GPa)	22.3	26.7	29.5	34.2	39.1
Lattice parameters (Å)	4.0176(4)	3.9958(4)	3.9798(6)	3.9583(5)	3.9387(5)
B position z	0.2002(22)	0.2010(42)	0.2001(51)	0.2002(47)	0.2007(46)
Reflections collected/unique	48/18	45/18	46/18	43/17	46/18
Rint	0.0375	0.0435	0.0390	0.0401	0.0568
Completeness (%)	81.8	81.8	81.8	85.0	85.7
Data/restraints/parameters	18/0/5	18/0/5	18/0/5	17/0/5	18/0/5
Goodness-of-fit on F^2	1.271	1.350	1.408	1.363	1.407
Final R indices R1	0.0125	0.0222	0.0182	0.0187	0.0191
wR2	0.0236	0.0547	0.0489	0.0402	0.0405
Largest diff. peak and hole (e/Å^3)	0.24/−0.38	0.48/−1.20	0.77/−0.52	0.50/−0.86	1.00/−0.52

[a]The 0.1 MPa data were collected outside the DAC.

Table 2. Parameters derived from the Birch–Murnaghan (BM) fit. Data from Ref. [8] was theoretical calculation results. Data of Ref. [6] was fitted with 2nd order BM equation, Ref. [17] and this work with 3rd order BM equation. Different pressure media (ME (methanol:ethanol=4:1), MEW (methanol:ethanol:water=16:3:1)) were used to provide quasi-hydrostatic conditions as presented in the table.

	Ref. [6]	Ref. [17]		Ref. [8]	This work
Pressure	ME	Ar	MEW		Ne
B_0	142±15	173±7	164±2	180	179±2
B_0'	4	4.2±1.5	4.0±0.4	3.79	3.6±0.1
Volume (Å^3)	71.68			71.34	71.89

The pressure–volume (P–V) curve obtained from ambient pressure to 39.1 GPa is shown in Fig. 1. The zero-pressure isothermal bulk modulus $B_0 = 179 \pm 2$ GPa and its pressure derivative $B_0' = 3.6 \pm 0.1$ were derived by fitting with the third-order Birch–Murnaghan equation of state (EOS) (Table 2).[27] The P–V EOS is compared with previous theoretical calculations and experimental results in Fig. 1. Our result is most consistent with the theoretical result.[8] All of the La–La, La–B, and B–B bond lengths decrease with increasing the pressure, and no abnormity is observed (Fig. 2). This confirms that there is no phase transition or structure change up to 39.1 GPa.

To investigate the work function and chemical bonds, the EDD was determined with the experimental structure factors by the RainbowMEM maximum entropy analysis package.[28] In the MEM calculation, the unit cell was divided into 48×48×48 pixels. In this work, the independent atom model (IAM) is used as the prior charge density. The IAM guarantees a good quality EDD.[29,30] The reliability factor of the MEM analysis $R_{\rm MEM}$ is less than 8%. The contour maps of the MEM electron densities for the (100) and (110) planes are shown in Fig. 3 with EDD from theoretical calculations by CASTEP. We use the Perdew, Burke and Ernzerh (PBE) exchange-correlation functional[31] to describe the exchange-correlation interaction. Energy cutoff of 600 eV and

$12 \times 12 \times 12$ Monkhorstpack grids of k points are found to be enough for convergence of quantities for LaB_6. The total energy is converged to within 5.0×10^{-6} eV/atom. At each pressure, we obtain a stable structure for geometry optimization. Here we classify two types of boron–boron bonds: B_6–B_6 and B–B. The B_6–B_6 bond represents the bond between two nearest octahedral atoms, whereas the B–B bond is the bond between the nearest atoms in the same octahedron. From the EDD results, both the B_6–B_6 and B–B bonds become stronger and shorter under high pressure. At ambient pressure, the electron density at the critical point (EDCP) values for B_6–B_6 and B–B are 0.46 and 0.52 e/Å^3, respectively (Fig. 4). As the pressure increases, the EDCP of the B_6–B_6 bond increases slightly faster than that of the B–B bond. At 39.1 GPa, the EDCP values of B_6–B_6 and B–B become 1.0 and 0.88 e/Å^3, respectively. Meanwhile, the electron densities of the La–La and La–B bonds remain at low levels, indicating that they remain ionic. The difference in the increasing rate of the EDCP between the B_6–B_6 and B–B bonds is because of the vibration of B atoms. The vibration orientation of B atoms is perpendicular to the inter-octahedral boron bonds. This type of vibration restrains the B_6–B_6 bond strength at ambient pressure. As the pressure increases, vibrations along this orientation weaken, while vibration along the inter-octahedral boron bonds becomes stronger. As a result, the B_6–B_6 bond is enhanced as the pressure increases and it is stronger than the B–B bond at high pressure.

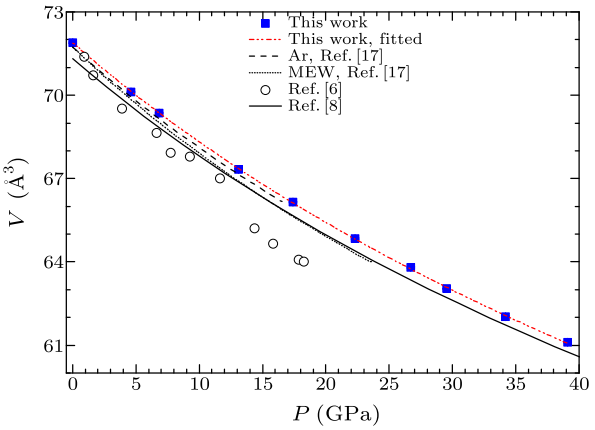

Fig. 1. Volume compression of LaB_6 at ambient temperature ($B_0 = 179(2)$ GPa and $B_0' = 3.6(1)$). The blue points are our data collected using neon as the pressure medium. The red line is the fitted line of our data. The dashed and dotted lines are the fits of the data from Ref. [17] with argon and methanol-ethanol-water (16:3:1) as the pressure medium, respectively. The circles are the data taken from Ref. [6] and the solid black line is the data taken from Ref. [8].

The work function W is the minimum energy required to move one electron from the Fermi energy (E_f) level to the vacuum energy (E_v) level: $W = E_v - E_f$, which is determined by the Fermi energy. In general, the compression strain can reduce the work functions of most metals.[32] Yutani *et al.* found that the film strain has a slight influence on the work function of LaB_6.[33] The work function of LaB_6 under ambient pressure has been investigated by experimental and theoretical methods.[1,33–37] Here we intend to characterize the change of the work function under pressure using highly accurate HPSXD data.

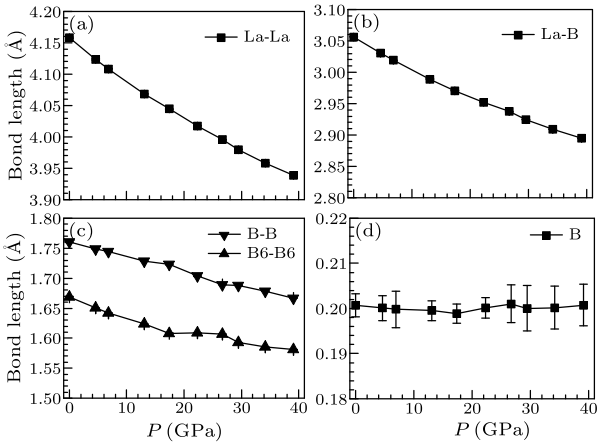

Fig. 2. The chemical bonds lengths measured at different pressures and 300 K: (a) La–La bond, (b) La–B bonds and (c) B–B and B6–B6 bond. (d) The internal parameter z of the boron atom position.

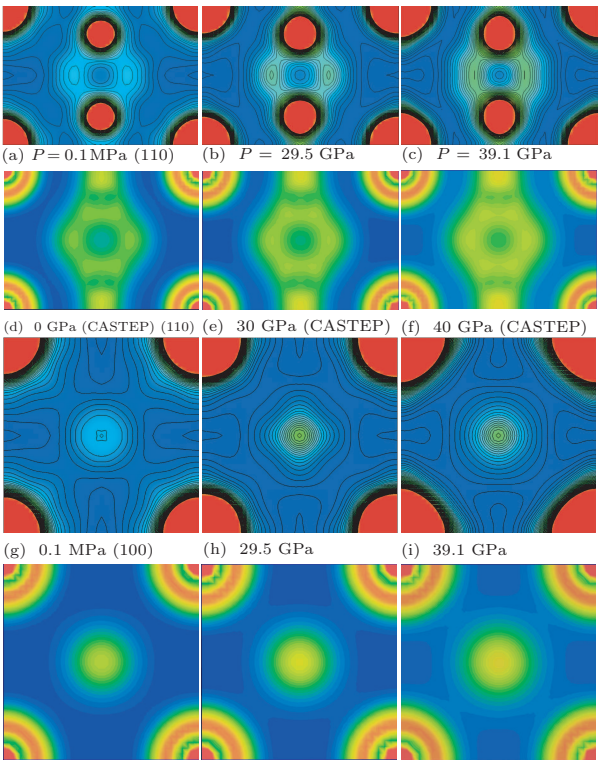

Fig. 3. EDD obtained by the MEM for the (110) plane (a)–(c) and the (100) plane (g)–(i). The contour lines are drawn from 0.1 to 2.0 e/Å^3 with a 0.05 e/Å^3 interval. Here (d)–(f) and (j)–(l) are the theoretical EDDs of the (110) and (100) planes from CASTEP, respectively, to show the reliability of our MEM results.

To investigate the work functions of the (100) and (110) planes under pressure, the theoretical work

function and EDD are calculated with the CASTEP package. We use the PBE exchange-correlation functional. The total energy is converged to within 5.0×10^{-6} eV/atom. With the experimental models, the work functions of LaB_6 (100) and (110) planes are calculated. The unit cells contain slabs with thicknesses of 6 and 4 bulk unit cells for (100) and (110) planes, respectively, and the vacuum thickness is set for 30 Å. Cutoff of 600 eV and k-point set of $12 \times 12 \times 1$ and $12 \times 8 \times 1$ are used for (100) and (110) planes, respectively. To simplify the calculations, all atom positions are restrained, in other words, no reconstructions are considered. The calculated work functions are shown in Fig. 5(c). The work function of the (110) plane decreases faster than that of the (100) plane in the high pressure range. The work function of the (100) surface remains at a relatively constant value.

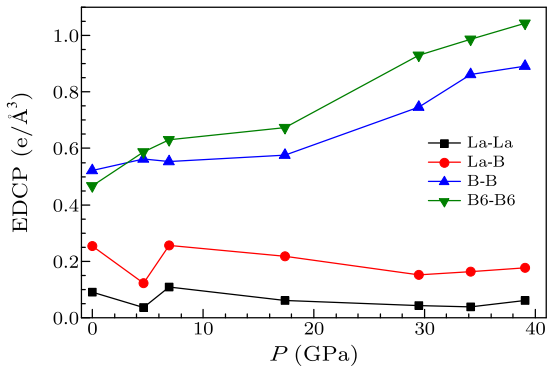

Fig. 4. EDCP results of the chemical bonds in the LaB_6 unit cell. Every bond is uniformly divided into 99 points. The average value of the five points closest to the saddle point is used to minimize the system error.

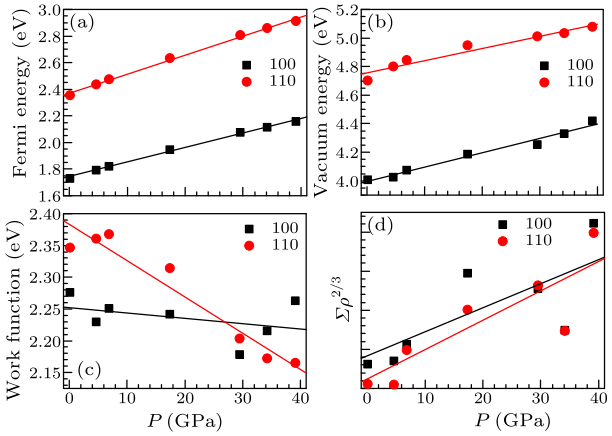

Fig. 5. (a) Fermi and (b) vacuum energy values of the (100) and (110) surfaces calculated with CASTEP using the experimental structure models. (c) Work functions of the (100) and (110) surfaces. (d) Experiment Fermi energies (represents values) of the (100) and (110) surfaces. Linear fitted lines are also shown.

From the EDD results, there are two types of chemical bonds in LaB_6: B–B and B_6–B_6 covalent bonds and La–La and La–B ionic bonds. When compressed, the rates of increase of the electron density of these two types of bonds are different. Figure 4 shows that the main contribution to the increase in the EDD comes from the covalent bonds. According to the Fermi–Dirac theory, the density of an ideal Fermi gas ρ is related to the Fermi vector k_f by $\rho = \frac{k_\mathrm{f}^3}{3\pi^2}$. With the Fermi energy $E_\mathrm{f} = \frac{\hbar^2 k_\mathrm{f}^2}{2m_\mathrm{e}}$, we can obtain

$$E_\mathrm{f} = \frac{(3\pi^2\rho)^{2/3}\hbar^2}{2m_\mathrm{e}}. \tag{1}$$

From Eq. (1), a higher rate of increase of ρ will produce a faster increase of E_f. In the LaB_6 crystal, the (100) surface only cuts one B_6–B_6 bond and one La–La bond, but the (110) surface cuts two B–B bonds. Therefore, the rate of increase of E_f for the (110) surface is higher than that for the (100) surface. As shown in Fig. 5(a), the fitted slope of the (110) surface is larger than that of the (100) surface.

The vacuum energy is described as the potential energy produced by the electrostatic potential

$$E_\mathrm{v} = V_{\rho_j} = \sum \frac{\rho_i \rho_j}{|\rho_i - \rho_j|}. \tag{2}$$

In the vacuum energy calculation, the volume of the crystal decreases with increasing the pressure. This produces an increase in the electronic density. Because the electrostatic potential can be expressed as $V \propto \rho/d$, where d is the distance from the crystal surface, both the vacuum energies of the (100) and (110) surfaces increase at almost the same rate, as shown in Fig. 5(b). Using $W = E_\mathrm{v} - E_\mathrm{f}$, the work functions of the two surfaces are calculated, as shown in Fig. 5(c). The properties of the LaB_6 work function for different planes under high pressures can be used as a guide for future applications of LaB_6.

With the experimental EDD, the Fermi energies of the (100) and (110) surfaces under different pressures can be easily calculated with Eq. (1). Figure 5(d) shows the experimental Fermi energy results. Figures 5(a) and 5(d) show that the slopes of the calculated and experimental results are consistent. This shows that with highly accurate experimental EDDs, the physical and chemical properties of materials can be directly investigated.

In conclusion, the structural and electronic stabilities of LaB_6 have been investigated with the aid of HPSXD data and the MEM method. No phase transition is observed up to 39.1 GPa. Furthermore, the work functions of the (110) and (100) surfaces under pressure have been investigated. The results show that the work function of the (110) surface slowly decreases, while the work function of the (100) surface remains at a relatively constant value with increasing the pressure. According to the EDD results, we believe that the different properties of the chemical bonds lead to different charge densities, and the different charge densities determine the different work functions under pressure.

We are grateful to Dr. Ligang Bai (Institute of High Energy Physics, CAS) for his help in preparing the manuscript. We thank Professor Jiuxing Zhang

(Beijing University of Technology, China) for supplying the LaB_6 sample.

References

[1] Uijttewaal M A, de Wijs G A and de Groot R A 2006 *J. Phys. Chem.* B **110** 18459
[2] Late D J, More M A, Joag D S, Misra P, Singh B and Kukreja L M 2006 *Appl. Phys. Lett.* **89** 123510
[3] Tanaka T, Yoshimoto J, Ishii M, Bannai E and Kawai S 1977 *Solid State Commun.* **22** 203
[4] Lundstrom T, Lonnberg B, Torma B, Etourneau J and Tarascon J M 1982 *Phys. Scr.* **26** 414
[5] Nakamura S, Goto T, Kasaya M and Kunii S 1991 *J. Phys. Soc. Jpn.* **60** 4311
[6] Teredesai P, Muthu D V S, Chandrabhas N, Meenakshi S, Vijayakumar V, Modak P, Rao R S, Godwal B K, Sikka S K and Sood A K 2004 *Solid State Commun.* **129** 791
[7] Baranovskiy A E, Grechnev G E, Fil V D, Ignatova T V, Logosha A V, Panfilov A S, Svechkarev I V, Shitsevalova N Y, Filippov V B and Eriksson O 2007 *J. Alloys Compd.* **442** 228
[8] Gürel T and Eryiğit R 2010 *Phys. Rev.* B **82** 104302
[9] Xu G, Chen J, Xia Y, Liu X, Liu Y and Zhang X 2009 *Chin. Phys. Lett.* **26** 056201
[10] Hasegawa A and Yanase A 1977 *J. Phys.* F **7** 1245
[11] Kubo Y and Asano S 1989 *Phys. Rev.* B **39** 8822
[12] Hossain F M, Riley D P and Murch G E 2005 *Phys. Rev.* B **72** 235101
[13] Bai L, Ma N and Liu F 2009 *Physica* B **404** 4086
[14] Duan J, Zhou T, Zhang L, Du J, Jiang G and Wang H 2015 *Chin. Phys.* B **24** 096201
[15] Kasai H and Nishibori E 2017 *Sci. Rep.* **7** 41375
[16] Chao L, Bao L, Wei W, O T and Zhang Z 2016 *J. Alloys Compd.* **672** 419
[17] Godwal B, Petruska E, Speziale S, Yan J, Clark S, Kruger M and Jeanloz R 2009 *Phys. Rev.* B **80** 172104
[18] Collins D M 1982 *Nature* **298** 49
[19] Casati N, Kleppe A, Jephcoat A P and Macchi P 2016 *Nat. Commun.* **7** 10901
[20] Li R, Liu J, Bai L, Tse J S and Shen G 2015 *Appl. Phys. Lett.* **107** 072109
[21] Tse J S, Hanfland M, Flacau R, Desgreniers S, Li Z, Mende K, Gilmore K, Nyrow A, Moretti Sala M and Sternemann C 2014 *J. Phys. Chem.* C **118** 1161
[22] Li X, Li H and Li P 2017 *Acta Phys. Sin.* **66** 036203 (in Chinese)
[23] Li X, Li H, Li P, Li R, Liu J, Li Y and Cui W 2017 *J. Synchrotron Rad.* **24** 699
[24] Mao H K, Xu J and Bell P M 1986 *J. Geophys. Res.: Solid Earth* **91** 4673
[25] Li H, Li X, He M, Li Y, Liu J, Shen G and Zhang Z 2013 *J. Appl. Crystallogr.* **46** 387
[26] Sheldrick G M 2008 *Acta Crystallogr. Sect.* A **64** 112
[27] Birch F 1947 *Phys. Rev.* **71** 809
[28] Li H, He M, Li J, Chen X and Zhang Z unpublished work
[29] de Vries R Y, Briels W J and Feil D 1996 *Phys. Rev. Lett.* **77** 1719
[30] van S and Netzel J 2009 *Phys. Scr.* **79** 048304
[31] Perdew J P, Burke K and Ernzerhof M 1996 *Phys. Rev. Lett.* **77** 3865
[32] Gong H R, Nishi Y and Cho K 2007 *Appl. Phys. Lett.* **91** 242105
[33] Yutani A, Kobayashi A and Kinbara A 1993 *Appl. Surf. Sci.* **70-71** 737
[34] Swanson L W and Dickinson T 1976 *Appl. Phys. Lett.* **28** 578
[35] Nishitani R, Aono M, Tanaka T, Oshima C, Kawai S, Iwasaki H and Nakamura S 1980 *Surf. Sci.* **93** 535
[36] Zhang H, Tang J, Yuan J, Ma J, Shinya N, Nakajima K, Murakami H, Ohkubo T and Qin L C 2010 *Nano Lett.* **10** 3539
[37] Monnier R and Delley B 2004 *Phys. Rev.* B **70** 193403